Inorganic Chemistry

Article

pubs.acs.org/IC

Structural Disorder in $AMoO_4$ (A = Ca, Sr, Ba) Scheelite Nanocrystals

Federico A. Rabuffetti,[†] Sean P. Culver,[†] Leopoldo Suescun,[‡] and Richard L. Brutchey*[,†]

[†]Department of Chemistry, University of Southern California, Los Angeles, California 90089, United States

[‡]Cryssmat−Lab/DETEMA, Facultad de Química, Universidad de la República, Montevideo, Uruguay

Supporting Information

ABSTRACT: The crystal structure of sub-15 nm $AMoO_4$ (A = Ca, Sr, Ba) scheelite nanocrystals has been investigated using a dual-space approach that combines Rietveld and pair distribution function (PDF) analysis of synchrotron X-ray diffraction data. Rietveld analysis yields an average crystal structure in which the Mo−O bond distance exhibits an anomalously large contraction (2.8%) upon chemical substitution of Ba^{2+} for Ca^{2+}. Such a dependence on chemical composition contradicts the well-known rigid character of Mo^{VI}−O bonds and the resulting rigidity of MoO_4 tetrahedra in scheelites. Unlike Rietveld, PDF analysis yields a local crystal structure in which the Mo−O bond distance shows a negligible contraction (0.4%) upon going from Ba^{2+} to Ca^{2+} and, therefore, appears independent of the chemical composition. Analysis of the anisotropic displacement parameters of the oxygen atom reveals that the disagreement between the average and local structural models arises from the presence of static orientational disorder of the MoO_4 tetrahedra. Rietveld analysis averages the random rotations of the MoO_4 tetrahedra across the scheelite lattice yielding an apparent Mo−O bond distance that is shorter than the true bond distance. In contrast, PDF analysis demonstrates that the structural integrity of the MoO_4 tetrahedra remains unchanged upon chemical substitution of the alkaline-earth cation, and that their orientational disorder is accommodated through geometric distortions of the AO_8 dodecahedra.

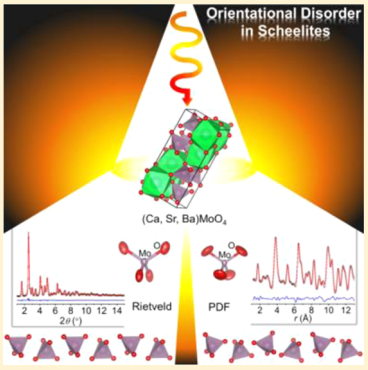

INTRODUCTION

Oxides with the formula AMO_4 (A = Ca, Sr, Ba; M = Mo, W) belonging to the scheelite family constitute an important class of functional materials in the areas of energy conversion and storage. Examples of applications include hosts for lanthanide ions in solid state phosphors[1] and lithium-ion batteries.[2,3] The archetypical $AMoO_4$ scheelite structure is shown in Figure 1. It features a tetragonal unit cell with space group $I4_1/a$ (Z = 4). Alkaline-earth and molybdenum atoms occupy special positions 4*a* (0, 1/4, 1/8) and 4*b* (0, 1/4, 5/8) respectively, whereas the oxygen atom sits in a general position 16*f* (*x*, *y*, *z*). The scheelite structure can be visualized as the assembly of AO_8 dodecahedra and MoO_4 tetrahedra. Each AO_8 dodecahedron is connected to four other dodecahedra through edge-sharing, resulting in zigzag chains that develop along the *c* axis. MoO_4 tetrahedra are isolated from each other and connected to AO_8 dodecahedra via bridging oxygen atoms; each oxygen atom is connected to two alkaline-earth atoms and one molybdenum atom. AO_8 dodecahedra are described by two distinct A−O distances and eight distinct O−A−O angles, while MoO_4 tetrahedra are described by a single Mo−O distance and two distinct O−Mo−O angles.[4] $CaMoO_4$, $SrMoO_4$, and $BaMoO_4$ form an isostructural series despite the large change in the ionic radius of the eight-coordinate alkaline-earth cation (rCa^{2+} = 1.12 Å, rSr^{2+} = 1.26 Å, and rBa^{2+} = 1.42 Å).[5]

Recently, our group reported the low temperature (<100 °C) synthesis of sub-15 nm $AMoO_4$ scheelite nanocrystals using the vapor diffusion sol−gel method.[6] Additionally, the crystal structure and lithium storage capacity of the nanocrystals were investigated using Rietveld analysis of conventional X-ray diffraction (XRD) data and galvanostatic cycling, respectively. Our work was motivated by the need to understand compositional control of structure−function relationships in nanocrystals of molybdenum-containing scheelites, as these have attracted attention as potential anode materials in lithium ion batteries.[3] Interestingly, an anomalously large contraction of the Mo−O bond distance in $AMoO_4$ nanocrystals was observed upon going from $CaMoO_4$ to $SrMoO_4$ and finally to $BaMoO_4$. This result was particularly surprising considering that Mo^{VI}−O bonds are known to be extremely rigid; as a consequence, MoO_4 tetrahedra in scheelites behave as nearly rigid units.[7−9] Structural changes induced by chemical substitution, in addition to pressure and temperature changes, are primarily accommodated through geometric distortions of the AO_8 dodecahedra, since A^{II}−O bonds are significantly more flexible due to their higher ionic character.[8,9] Herein, we report an in-depth structural investigation of sub-15 nm $AMoO_4$ scheelite nanocrystals using a dual-space approach that combines Rietveld and pair distribution function (PDF) analysis of synchrotron XRD data. Comparison of the average and local crystal structures shows that the anomalous contraction of the Mo−O bond distance observed by Rietveld analysis originates from static orientational disorder of the MoO_4 tetrahedra across the scheelite lattice. The significance of coupling Rietveld and

Received: October 7, 2013
Published: November 22, 2013

   dx.doi.org/10.1021/ic4025348 | *Inorg. Chem.* 2014, 53, 1056−1061

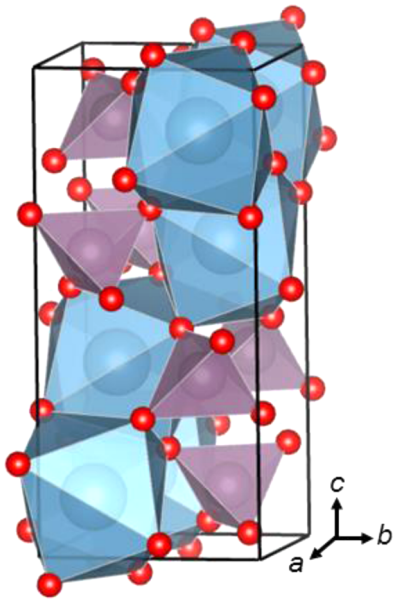

Figure 1. $AMoO_4$ scheelite structure (A = Ca, Sr, Ba). Blue, purple, and red spheres represent alkaline-earth, molybdenum, and oxygen atoms, respectively.

PDF analysis to achieve an accurate description of the atomic arrangement in nanocrystals is highlighted.

EXPERIMENTAL SECTION

Synthesis of $AMoO_4$ Nanocrystals. $AMoO_4$ nanocrystals were synthesized via a vapor diffusion sol–gel method described in detail elsewhere.[6] Briefly, $MoO_2(acac)_2$ (95%; Sigma Aldrich) was dissolved in the corresponding $A(OR)_2$ alkoxide (R = $CH_2CH_2OCH_3$ for Ca and $CH_2CHCH_3OCH_3$ for Sr and Ba; Gelest, Inc.) in a 1:1 molar ratio. The resulting solution was exposed to a controlled flow of water vapor for 48 h at room temperature and atmospheric pressure. Diffusion of water vapor into the solution resulted in the formation of a cracked gel, which was subsequently aged under a nitrogen atmosphere for 24 h at 80 °C. The resulting gel was collected, washed with absolute ethanol (3 × 10 mL), and vacuum-dried at room temperature to recover an off-white fine powder consisting of $AMoO_4$ nanocrystals. TEM analysis revealed that these nanocrystals exhibited a quasispherical shape with an average diameter of 9.3 ± 2.7, 7.9 ± 1.9, and 12.3 ± 2.8 nm for $CaMoO_4$, $SrMoO_4$, and $BaMoO_4$, respectively.[6]

Synchrotron X-ray Diffraction. X-ray diffraction patterns were collected at the 11–ID–B beamline of the Advanced Photon Source at Argonne National Laboratory. An incident photon energy of 90.484 keV (λ = 0.137024 Å) was employed. Samples were loaded in Kapton tubes and diffraction data were collected in transmission mode at room temperature.

Rietveld Analysis. Rietveld structural refinements were carried out using the GSAS software.[10,11] Experimental data and atomic X-ray scattering factors were corrected for sample absorption and anomalous scattering, respectively. The average crystal structure of $AMoO_4$ nanocrystals was refined with the tetragonal $I4_1/a$ space group. The following parameters were refined: (1) scale factor, (2) background, which was modeled using a shifted Chebyschev polynomial function, (3) peak shape, which was modeled using a modified Thomson–Cox–Hastings pseudo-Voigt function,[12] (4) lattice constants (a and c), (5) fractional atomic coordinates of the oxygen atom (x_O, y_O, z_O), and (6) atomic anisotropic displacement parameters constrained by the site symmetry (U^{11} and U^{33} for Ca, Sr, Ba, and Mo, and U^{11}, U^{22}, U^{33}, U^{12}, U^{13}, and U^{23} for O). The R_{wp} indicator was employed to assess the quality of the refined structural models.[13]

Pair Distribution Function Analysis. The pair distribution function $G(r)$ defined as:

$$G(r) = 4\pi r[\rho(r) - \rho_0] = (2/\pi)\int_Q^{Q_{max}} Q[S(Q) - 1]\sin(Qr)dQ$$

was employed for structural analysis. Here, r is the radial distance, $\rho(r)$ and ρ_0 are the local and average atomic number density, respectively, and Q is the magnitude of scattering vector. The RAD software was employed to extract $G(r)$ from the raw diffraction data.[14] These were first corrected for background, sample absorption, and Compton scattering. Then, normalized structure functions $S(Q)$ were obtained; these are given in the Supporting Information. Finally, $S(Q)$ was Fourier-transformed to yield $G(r)$. A maximum scattering vector

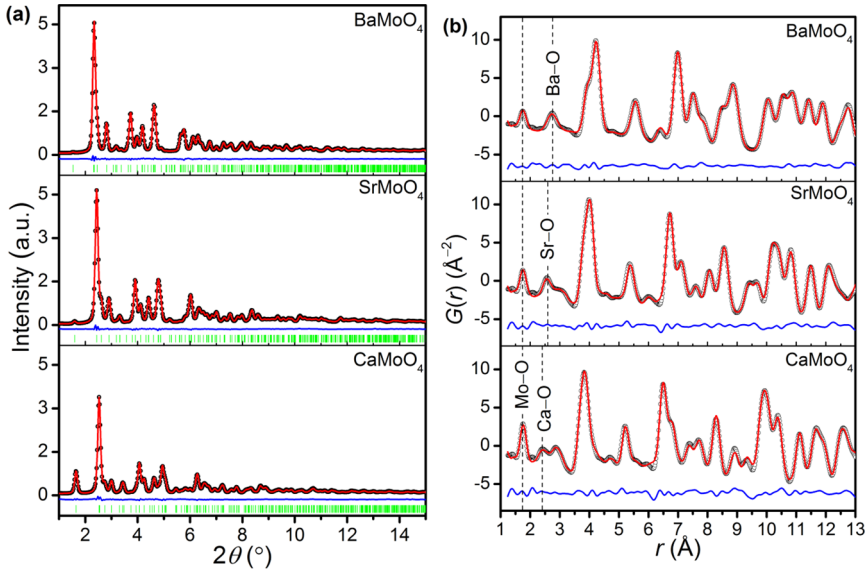

Figure 2. (a) Rietveld and (b) PDF analysis of the XRD patterns of $AMoO_4$ nanocrystals. Experimental (○) and calculated (red) patterns are shown along with the difference curve (blue). Tickmarks (green) corresponding to the phase refined are given in a, and PDF peaks arising from A–O and Mo–O pairs are indicated in b. Note the Mo–O interatomic distance does not change with chemical composition. Difference curves in b have been offset for clarity.

dx.doi.org/10.1021/ic4025348 | Inorg. Chem. 2014, 53, 1056–1061

(Q_{max}) of 25 Å^{-1} was employed in the Fourier transform. Structural refinements were carried out using the PDFgui software.[15] The local crystal structure of $AMoO_4$ nanocrystals was refined with the tetragonal $I4_1/a$ space group. Fits of this structural model to the experimental PDFs were performed in the 1.25−13 Å interatomic distance range in order to account for all atom−atom pairs along the largest dimension of the unit cell. The following parameters were refined: (1) scale factor, (2) lattice constants (a and c), (3) fractional atomic coordinates of the oxygen atom (x_O, y_O, z_O), and (4) atomic anisotropic displacement parameters constrained by the site symmetry (U^{11} and U^{33} for Ca, Sr, Ba, and Mo, and U^{11}, U^{22}, U^{33}, U^{12}, U^{13}, and U^{23} for O). The R_w indicator was employed to assess the quality of the refined structural models.[16]

Bond Distance Distortion Index. The bond distance distortion index[17] (Δ_{AO_8}) was employed to quantitatively assess geometric distortions of the AO_8 dodecahedra. Δ_{AO_8} is defined as:

$$\Delta_{AO_8} = \frac{1}{8}\sum_{i=1}^{8}\frac{|d^i_{A-O} - \langle d_{A-O}\rangle|}{\langle d_{A-O}\rangle}$$

where $\langle d_{A-O}\rangle$ is the average A−O bond distance.

RESULTS AND DISCUSSION

Rietveld and PDF fits to the experimental XRD patterns of $AMoO_4$ nanocrystals are shown in Figure 2. Calculated structural parameters are given in Tables 1 and 2. Bond lengths, bond angles, and bond distance distortion indices are given in Tables 3 and 4. Calculated lattice constants a and $c/2$, and A−O and Mo−O bond distances are plotted in Figure 3 as function of the ionic radius of the alkaline-earth cation. Low R_{wp} and R_w values and visual inspection of the fits show that both the average and local crystal structure of $AMoO_4$ nanocrystals are adequately described by a tetragonal scheelite structure with space group $I4_1/a$. It is worth noting that R_w values below 10% were obtained for the fits to the experimental PDFs, whereas typical R_w values reported in the literature range from 10 to 25%, depending on the chemical nature of the material and its form factor. In addition, inspection of Tables 1 and 2 reveals that a complete set of physically plausible structural parameters can be extracted from the experimental XRD patterns using both Rietveld and PDF analysis. Important in the context of this investigation is the fact that positively defined anisotropic mean-square displacements were obtained for the oxygen atom in all cases (vide infra). Rietveld and PDF analysis show the $AMoO_4$ unit cell axes expand linearly upon going from $CaMoO_4$ to $BaMoO_4$, as expected on the basis of

Table 1. Structural Parameters of $AMoO_4$ Nanocrystals Extracted From Rietveld Analysis

		$CaMoO_4$	$SrMoO_4$	$BaMoO_4$
a (Å)		5.2334(6)	5.4039(4)	5.5871(4)
c (Å)		11.4477(15)	12.0392(10)	12.8223(11)
c/a		2.19(4)	2.23(2)	2.29(2)
V (Å^3)		313.53(8)	351.57(6)	400.26(7)
x_O		0.6462(7)	0.6337(7)	0.6171(10)
y_O		0.5103(6)	0.5188(7)	0.5289(11)
z_O		0.2080(4)	0.2048(4)	0.2006(5)
A:	U^{11a} (Å^2)	0.74(11)	1.24(12)	1.82(12)
	U^{33} (Å^2)	1.22(18)	1.03(19)	1.23(16)
	U_{eq} (Å^2)	0.90(8)	1.17(8)	1.62(8)
Mo:	U^{11} (Å^2)	0.80(5)	0.44(9)	0.35(11)
	U^{33} (Å^2)	0.90(8)	0.75(16)	0.58(16)
	U_{eq} (Å^2)	0.83(4)	0.54(7)	0.42(8)
O:	U^{11} (Å^2)	1.1(3)	1.2(3)	1.7(2)
	U^{22} (Å^2)	1.2(3)	2.5(3)	4.1(5)
	U^{33} (Å^2)	2.6(4)	2.1(3)	2.4(5)
	U^{12} (Å^2)	−0.2(2)	−0.9(3)	0.6(4)
	U^{13} (Å^2)	0.2(2)	0.6(2)	0.6(3)
	U^{23} (Å^2)	−0.5(2)	0.2(2)	0.7(4)
	U_{eq} (Å^2)	1.62(19)	1.95(17)	2.7(2)
R_{wp} (%)		2.8	2.2	2.0

[a]Atomic displacements parameters are given as 100 × U^{ij}.

Table 2. Structural Parameters of $AMoO_4$ Nanocrystals Extracted From PDF Analysis

		$CaMoO_4$	$SrMoO_4$	$BaMoO_4$
a (Å)		5.220(2)	5.390(2)	5.571(3)
c (Å)		11.407(10)	12.000(10)	12.783(10)
c/a		2.19(20)	2.23(20)	2.30(20)
V (Å^3)		310.8(4)	348.5(4)	396.7(5)
x_O		0.642(4)	0.630(5)	0.605(11)
y_O		0.507(3)	0.514(5)	0.512(8)
z_O		0.212(2)	0.208(3)	0.204(4)
A:	U^{11a} (Å^2)	0.9(2)	0.9(8)	1.2(6)
	U^{33} (Å^2)	1.5(6)	1.0(1.7)	1.1(9)
	U_{eq} (Å^2)	1.1(2)	0.9(7)	1.2(4)
Mo:	U^{11} (Å^2)	0.70(10)	1.1(8)	1.2(7)
	U^{33} (Å^2)	0.90(2)	1.1(1.7)	1.0(1.2)
	U_{eq} (Å^2)	0.76(8)	1.1(7)	1.1(5)
O:	U^{11} (Å^2)	3.8(1.1)	3.4(1.8)	13(7)
	U^{22} (Å^2)	3.4(1.2)	9(4)	9(5)
	U^{33} (Å^2)	2.5(9)	4.1(1.9)	2(3)
	U^{12} (Å^2)	0.2(7)	−2.2(1.8)	1.3(7)
	U^{13} (Å^2)	−0.8(6)	−2.0(1.4)	2.7(3)
	U^{23} (Å^2)	0.16(7)	2.5(1.7)	2(2)
	U_{eq} (Å^2)	3(1)	5(2)	8(3)
R_w (%)		9.7	8.3	7.0

[a]Atomic displacements parameters are given as 100 × U^{ij}.

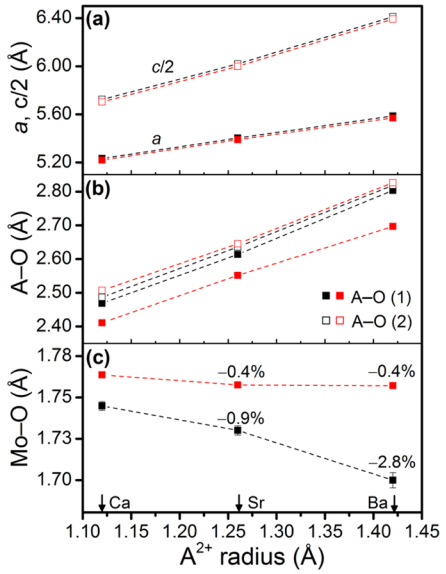

Figure 3. (a) Lattice constants a and $c/2$, (b) A−O bond distances, and (c) Mo−O bond distance extracted from Rietveld (black symbols) and PDF (red symbols) analysis of the XRD patterns of $AMoO_4$ nanocrystals. The percent contraction of the Mo−O bond distance in $SrMoO_4$ and $BaMoO_4$ relative to $CaMoO_4$ is indicated in c. Dashed lines are guides for the eye.

dx.doi.org/10.1021/ic4025348 | Inorg. Chem. 2014, 53, 1056−1061

the ionic radii (Figure 3a). This expansion is slightly anisotropic and occurs primarily along the *c* axis. As a result, the metrics of the tetragonal unit cell changes: the *c*/*a* ratio increases from 2.19 to 2.30 (Tables 1 and 2). The increased sensitivity of the *c* axis to chemical composition, temperature, and pressure changes has been extensively reported in structural studies of bulk $AMoO_4$.[7−9] Rietveld and PDF analysis also give a similar description of the evolution of the two distinct A−O bond distances (denoted as A-O (1) and A-O (2) in Figure 3b) with chemical composition. Both increase linearly and at the same rate upon going from $CaMoO_4$ to $BaMoO_4$ (Figure 3b). According to Rietveld (PDF) analysis, the average A−O distance increases by 13−14% (12−13%). Interestingly, however, the bond distance distortion of the AO_8 dodecahedra appears much larger to PDF than to Rietveld analysis, regardless of the chemical composition (Tables 3 and 4). Bond distance distortion values in the 18−24 range are obtained using the latter, while values in the 2.7−4.2 range are obtained using the former. In other words, the AO_8 dodecahedra appear more distorted on the local scale. When it comes to the description of the evolution of the Mo−O distance with chemical composition, both Rietveld and PDF analysis reveal a contraction upon going from $CaMoO_4$ to $BaMoO_4$ (Figure 3c). As a result, the volume of the MoO_4 tetrahedra decreases (Tables 3 and 4). Thus, the expansion of the unit cell observed upon increasing the ionic radius of the alkaline-earth cation is driven by the expansion of the AO_8 dodecahedra. However, the Mo−O distance derived from Rietveld analysis shows an abnormally large contraction of 2.8% upon going from $CaMoO_4$ to $BaMoO_4$. In contrast, the bond distance derived from PDF analysis shows a negligible contraction of 0.4%, in agreement with the well-known rigidity of MoO_4 tetrahedra in $AMoO_4$ scheelites.[8,9] This is clearly noticeable in Figure 2b, where the peak corresponding to the Mo−O pair remains at the same *r* value (∼1.76 Å) for $CaMoO_4$, $SrMoO_4$, and $BaMoO_4$.

To further explore similarities and differences between the structural models derived from Rietveld and PDF analysis, we calculated bond valence sums (BVS)[18] using A−O and Mo−O bond distances extracted from both approaches, and corresponding results are given in Table 5. For comparison, we have included BVSs reported by Nassif et al. in a combined powder X-ray and neutron diffraction investigation of bulk $BaMoO_4$ synthesized via solid state reaction.[19] These authors also computed BVSs using structural parameters derived by Gurmen et al. and Hazen et al. in their structural investigations of single crystal $CaMoO_4$ and $SrMoO_4$.[4,7] The common features observed in these structural investigations are the overbonded and underbonded character of the alkaline-earth and molybdenum cations, respectively, as well as the increasing strength of the Mo−O bond upon increasing the radius of the alkaline-earth cation. This crystallochemical picture for the bulk materials has been validated by studying the relative thermal stabilities of $CaMoO_4$, $SrMoO_4$, and $BaMoO_4$ against reduction under hydrogen atmosphere.[19,20] Interestingly, BVSs derived from PDF analysis of $AMoO_4$ nanocrystals are in excellent agreement with those reported for their bulk counterparts, indicating the corresponding structural models are adequate. In contrast, BVSs derived from Rietveld analysis yield an overbonded character for the molybdenum atom, suggesting

Table 3. Bond Angles, Bond Distances, and Polyhedra Distortion Indices Extracted From Rietveld Analysis

	$CaMoO_4$	$SrMoO_4$	$BaMoO_4$
AO_8			
A−O (Å)	2.469(4)	2.614(4)	2.804(6)
	2.487(4)	2.636(4)	2.819(5)
O−A−O (deg)	151.18(15)	148.77(15)	145.6(2)
	68.46(9)	67.41(10)	66.14(13)
	98.39(6)	97.62(6)	96.78(6)
	73.46(6)	73.51(6)	73.94(9)
	135.10(17)	137.28(17)	139.8(2)
	77.05(10)	79.22(10)	81.72(15)
	126.85(11)	127.95(12)	129.54(18)
	78.50(18)	76.71(19)	74.2(3)
V_{AO_8} (Å^3)	27.07	32.22	39.49
Δ_{AO_8} (× 10^3)	3.6	4.2	2.7
MoO_4			
Mo−O (Å)	1.750(3)	1.734(3)	1.701(5)
O−Mo−O (deg)	107.14(14)	107.87(14)	108.9(2)
	114.2(3)	112.7(3)	110.5(4)
V_{MoO_4} (Å^3)	2.74	2.67	2.53

Table 4. Bond Angles, Bond Distances, and Polyhedra Distortion Indices Extracted From PDF Analysis

	$CaMoO_4$	$SrMoO_4$	$BaMoO_4$
AO_8			
A−O (Å)	2.4112(13)	2.5518(14)	2.6967(13)
	2.5071(10)	2.6456(10)	2.8266(10)
O−A−O (deg)	152.2(3)	149.7(3)	145.4(4)
	68.0(3)	67.1(3)	66.4(4)
	99.0(3)	98.2(3)	97.3(4)
	74.0(3)	74.3(4)	75.8(4)
	133.5(3)	135.6(4)	138.3(4)
	76.4(3)	78.3(3)	79.8(4)
	126.6(3)	127.9(3)	131.3(4)
	79.0(3)	76.7(4)	71.4(4)
V_{AO_8} (Å^3)	26.49	31.33	37.72
Δ_{AO_8} (× 10^3)	19.5	18.0	23.5
MoO_4			
Mo−O (Å)	1.7698(7)	1.7632(7)	1.7627(7)
O−Mo−O (deg)	108.3(4)	108.7(5)	109.0(6)
	111.9(4)	111.0(5)	110.4(6)
V_{MoO_4} (Å^3)	2.84	2.81	2.81

Table 5. Bond Valence Sums in $AMoO_4$ Nanocrystals

		A[a]	Mo[a]	O[a]
$CaMoO_4$	Rietveld	2.01	6.12	2.03
	PDF	2.13	5.80	1.98
	Rietveld in bulk[b]	2.12	5.78	1.98
$SrMoO_4$	Rietveld	2.03	6.40	2.11
	PDF	2.20	5.90	2.02
	Rietveld in bulk[b]	2.19	5.84	2.01
$BaMoO_4$	Rietveld	1.93	6.98	2.23
	PDF	2.40	5.91	2.04
	Rietveld in bulk[b]	2.37	5.88	2.06

[a]Bond valence parameters l_0 for Ca (1.967), Sr (2.118), Ba (2.285), and Mo (1.907) were taken from ref 18. The empirical constant *b* was fixed at 0.37. [b]Ref 19.

dx.doi.org/10.1021/ic4025348 | Inorg. Chem. 2014, 53, 1056−1061

the corresponding structural models fail to accurately describe Mo−O bonds within the MoO_4 tetrahedra.

Results presented thus far demonstrate that PDF analysis provides a crystallochemically sensible description of Mo−O bonds in $AMoO_4$ nanocrystals, whereas Rietveld analysis does not. The origin of this deficiency can be understood by inspecting the shape and orientation of the thermal ellipsoids of the oxygen atoms as a function of the chemical composition (Figure 4). Thermal ellipsoids extracted from Rietveld analysis

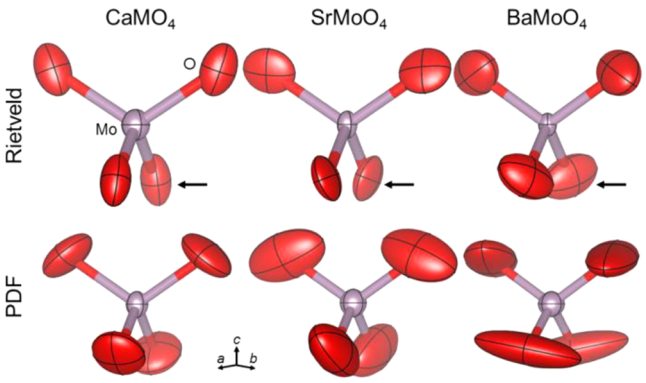

Figure 4. MoO_4 tetrahedra in $AMoO_4$ nanocrystals as described by Rietveld (top) and PDF (bottom) analysis of XRD data. Thermal ellipsoids are drawn with a 95% probability. Ellipsoids derived from Rietveld analysis exhibit a component perpendicular to the Mo−O bond that increases upon going from $CaMoO_4$ to $BaMoO_4$. This change is best observed by looking at the ellipsoid indicated with an arrow. In contrast, the largest component of the ellipsoids derived from PDF analysis appears perpendicular to the Mo−O bond, regardless of the chemical composition.

change their shape and orientation relative to the Mo−O bond upon going from $CaMoO_4$ to $BaMoO_4$. The component of the ellipsoid perpendicular to the Mo−O bond increases from $CaMoO_4$ to $BaMoO_4$. In contrast, ellipsoids derived from PDF analysis appear elongated along a direction perpendicular to the Mo−O bond, regardless of the chemical composition. This observation explains why the Mo−O bond distance extracted from Rietveld analysis is significantly shorter than that provided by PDF analysis and why this disagreement becomes more noticeable upon going from $CaMoO_4$ to $SrMoO_4$ and finally to $BaMoO_4$. An ellipsoid elongated perpendicular to the Mo−O bond axis leads to an apparent bond distance that is shorter than the true bond distance, because the projection of the local position of the oxygen onto the direction that connects the molybdenum with the average position of the oxygen is shorter than the actual bond distance. This effect is similar to libration,[21] but in our case its origin appears to be mainly static rather than dynamic as discussed hereafter. Indeed, the PDF peak corresponding to the Mo−O pair features a nearly constant full width at half-maximum: values of 0.19, 0.19, and 0.20 Å were obtained for $CaMoO_4$, $SrMoO_4$, and $BaMoO_4$, respectively, upon fitting the Mo−O peak with a single Gaussian. This observation and the nearly constant Mo−O bond distance demonstrate that the dynamics and structural integrity of the MoO_4 tetrahedra does not change significantly with chemical composition. In addition, the disagreement between the average and local structural models provided by Rietveld and PDF analysis, respectively, would not be such if the effect responsible for it was dynamic in nature. Considered all together, these findings indicate the presence of static disorder in $AMoO_4$ scheelite nanocrystals. Specifically, they point to orientational disorder of the MoO_4 tetrahedra; that is, these tetrahedra are randomly rotated throughout the scheelite lattice. Rietveld analysis averages this orientational disorder yielding a structural model that differs from that provided by PDF analysis, which probes the local crystal structure. The presence of disorder in $AMoO_4$ nanocrystals was further confirmed by fits of the proposed structural model to the experimental PDFs in the 1.25−80 Å interatomic distance range (see the Supporting Information). For these fits, R_w values of 14.5, 14.5, and 12.0% were obtained for $CaMoO_4$, $SrMoO_4$, and $BaMoO_4$, respectively. These are systematically larger than those obtained in fits performed in the 1.25−13 Å interatomic distance range, thus reflecting the loss of coherence in the assembly of AO_8 and MoO_4 polyhedra as atomic pairs that are further apart are incorporated into the structural refinement. Orientational disorder in $AMoO_4$ scheelites is not surprising considering these are open framework structures that have a high degree of structural flexibility. Specifically in the case of MoO_4 tetrahedra, these share corners with neighboring AO_8 dodecahedra via a bridging oxygen atom. The presence of A−O−Mo "hinges" provides the tetrahedra with significant rotational freedom.[21] A similar structural flexibility, coupled with transverse lattice vibrations, is at the origin of the negative thermal expansion (NTE) coefficients exhibited by oxides containing $(Mo,W)O_4$ and $(Mo,W)O_6$ corner-sharing polyhedra.[21−24] Unlike NTE materials, however, MoO_4 tetrahedra in $AMoO_4$ nanocrystals did not show any signs of concerted rotation. The hypothesis of orientational disorder can also be invoked to explain the observation that AO_8 dodecahedra appear more distorted on the local scale. Indeed, such an observation results from the fact that random rotations of MoO_4 tetrahedra are primarily accommodated through geometric distortions of the AO_8 dodecahedra rather than by affecting the structural integrity of the tetrahedra, as expected on the basis of the relative rigidities of the A−O and Mo−O bonds.[9]

Finally, we comment on the significance of coupling Rietveld and PDF analysis to achieve an accurate representation of the atomic arrangement in nano- and microcrystals. Results presented herein demonstrate the inability of Rietveld analysis to provide a fully consistent crystallochemical description of $AMoO_4$ nanocrystals. This limitation of the Rietveld method arises from the reduced structural coherence of nanocrystals relative to their bulk counterparts. Petkov et al. have shown that the reduction of structural coherence in spatially confined chemical systems results from an enhancement of atomic positional disorder.[25] As mentioned earlier, the structural flexibility of $AMoO_4$ scheelites is intrinsic to their crystal structure. Thus, it seems reasonable to assume that orientational disorder of the MoO_4 tetrahedra occurs in both bulk and nanocrystalline form factors. The fact that Rietveld analysis provides an adequate structural model for $AMoO_4$ in bulk form[19] but not in nanocrystalline form, indicates that random rotations of the MoO_4 tetrahedra occur to a much larger extent in the latter, merely reflecting their enhanced atomic positional disorder. Indeed, Nogueira and co-workers recently suggested the presence of structural disorder in $Ba_{1-x}Sr_xMoO_4$ microcrystals synthesized by a coprecipitation method.[26] However, the use of Rietveld analysis as the unique quantitative probe of the crystal structure prevented them from identifying the exact origin and nature of the disorder. This observation, coupled to results presented herein, demonstrates the significance of

dx.doi.org/10.1021/ic4025348 | Inorg. Chem. 2014, 53, 1056−1061

combining Rietveld and PDF analysis to achieve an accurate description of the atomic arrangement in both nano- and microcrystals of materials in which local structural distortions are expected to occur.

CONCLUSIONS

In summary, the average and local crystal structures of sub-15 nm $AMoO_4$ scheelite nanocrystals were investigated by employing a dual-space approach that combined Rietveld and PDF analysis of synchrotron XRD data. The latter method yielded a crystallochemically consistent structural model, whereas the former failed to accurately describe the dependence of the Mo−O bond distance with chemical composition. Specifically, an anomalously large contraction of the Mo−O bond distance was observed in the structural model derived from Rietveld analysis upon increasing the ionic radius of the alkaline-earth cation. However, a negligible contraction was observed in the structural model extracted via PDF analysis. The apparent contradiction between both models can be reconciled by invoking the presence of static orientational disorder of the MoO_4 tetrahedra. Rietveld analysis averages the random rotations of the tetrahedra across the scheelite lattice, thereby yielding an apparent Mo−O bond distance that is shorter than the true bond distance. In contrast, PDF analysis shows these random rotations are accommodated mainly through geometric distortions of the AO_8 dodecahedra, whereas the structural integrity of the MoO_4 tetrahedra remains unchanged upon chemical substitution of the alkaline-earth cation. From a methodological standpoint, results presented herein show the significance of employing a dual-space approach that combines Rietveld and PDF analysis to identify local structural distortions in nanocrystals from a single diffraction measurement.

ASSOCIATED CONTENT

Supporting Information

Structure functions $S(Q)$; fits to the experimental PDFs of $AMoO_4$ nanocrystals in the 1.25−80 Å interatomic distance range. This material is available free of charge via the Internet at http://pubs.acs.org.

AUTHOR INFORMATION

Corresponding Author

*E-mail: brutchey@usc.edu.

Notes

The authors declare no competing financial interest.

ACKNOWLEDGMENTS

This material is based on work supported by the Department of Energy Office of Basic Energy Sciences under Grant DE−FG02−11ER46826. S.P.C. acknowledges the National Science Foundation for a Graduate Research Fellowship. The authors thank Dr. Karena Chapman and Dr. Kevin Beyer from the 11−ID−B beamline of the Advanced Photon Source for their assistance with the collection of X-ray diffraction data. Use of the Advanced Photon Source at Argonne National Laboratory was supported by the U.S. Department of Energy, Office of Science, Office of Basic Energy Sciences, under Contract DE−AC02−06CH11357.

REFERENCES

(1) Senyshyn, A.; Hoelzel, M.; Hansen, T.; Vasylechko, L.; Mikhailik, V.; Kraus, H.; Ehrenberg, H. *J. Appl. Crystallogr.* **2011**, *44*, 319−326.
(2) Sharma, N.; Shaju, K. M.; Subba Rao, G. V.; Chowdari, B. V. R.; Dong, Z. L.; White, T. J. *Chem. Mater.* **2004**, *16*, 504−512.
(3) Reddy, M. V.; Subba Rao, G. V.; Chowdari, B. V. R. *Chem. Rev.* **2013**, *113*, 5364−5457.
(4) Gurmen, E.; Daniels, E.; King, J. S. *J. Chem. Phys.* **1971**, *55*, 1093−1097.
(5) Shannon, R. D. *Acta Crystallogr., Sect. A* **1976**, *32*, 751−767.
(6) Culver, S. P.; Rabuffetti, F. A.; Zhou, S.; Mecklenburg, M.; Song, Y.; Melot, B. C.; Brutchey, R. L. *Chem. Mater.* **2013**, *25*, 4129−4134.
(7) Hazen, R. M.; Finger, L. W.; Mariathasan, J. W. E. *J. Phys. Chem. Solids* **1985**, *46*, 253−263.
(8) Achary, S. N.; Patwe, S. J.; Mathews, M. D.; Tyagi, A. K. *J. Phys. Chem. Solids* **2006**, *67*, 774−781.
(9) Errandonea, D.; Kumar, R. S.; Ma, X.; Tu, C. *J. Solid State Chem.* **2008**, *181*, 355−364.
(10) Larson, A. C.; Von Dreele, R. B. *General Structure Analysis System (GSAS)*; Los Alamos National Laboratory: Los Alamos, NM, 2000.
(11) Toby, B. H. *J. Appl. Crystallogr.* **2011**, *34*, 210−213.
(12) Thompson, P.; Cox, D. E.; Hastings, J. M. *J. Appl. Crystallogr.* **1987**, *20*, 79−83.
(13) Young, R. A. *The Rietveld Method*; Oxford University Press: New York, 1993.
(14) Petkov, V. *J. Appl. Crystallogr.* **1989**, *22*, 387−389.
(15) Farrow, C. L.; Juhas, P.; Liu, J. W.; Bryndin, D.; Bozin, E. S.; Bloch, J.; Proffen, T.; Billinge, S. J. L. *J. Phys.: Condens. Matter* **2007**, *19*, 335219.
(16) Petkov, V.; Gateshki, M.; Niederberger, M.; Ren, Y. *Chem. Mater.* **2006**, *18*, 814−821.
(17) Baur, W. H. *Acta Crystallogr.* **1974**, *B30*, 1195−1215.
(18) Brese, N. E.; O'Keeffe, M. *Acta Crystallogr.* **1991**, *B47*, 192−197.
(19) Nassif, V.; Carbonio, R. E.; Alonso, J. A. *J. Solid State Chem.* **1999**, *146*, 266−270.
(20) Kamata, K.; Nakamura, T.; Sata, T. *Mater. Res. Bull.* **1975**, *10*, 373−378.
(21) Miller, W.; Smith, C. W.; Mackenzie, D. S.; Evans, K. E. *J. Mater. Sci.* **2009**, *44*, 5441−5451.
(22) Evans, J. S. O.; Mary, T. A.; Vogt, T.; Subramanian, M. A.; Sleight, A. W. *Chem. Mater.* **1996**, *8*, 2809−2823.
(23) Mittal, R.; Chaplot, S. L.; Schober, H.; Kolesnikov, A. I.; Loong, C.-K.; Lind, C.; Wilkinson, A. P. *Phys. Rev. B* **2004**, *70*, 214303.
(24) Lind, C. *Materials* **2012**, *5*, 1125−1154.
(25) Petkov, V.; Buscaglia, V.; Buscaglia, M. T.; Zhao, Z.; Ren, Y. *Phys. Rev. B* **2008**, *78*, 054107.
(26) Nogueira, I. C.; Cavalcante, L. S.; Pereira, P. F. S.; de Jesus, M. M.; Rivas Mercury, J. M.; Batista, N. C.; Siu, L. M.; Longo, E. *J. Appl. Crystallogr.* **2013**, *46*, 1434−1446.